Inorganic Chemistry

ARTICLE

pubs.acs.org/IC

Copper(I) Thiocyanate-Amine Networks: Synthesis, Structure, and Luminescence Behavior.

Kayla M. Miller, Shannon M. McCullough, Elena A. Lepekhina, Isabelle J. Thibau, and Robert D. Pike*

Department of Chemistry, College of William and Mary, Williamsburg, Virginia 23187-8795, United States

Xiaobo Li, James P. Killarney, and Howard H. Patterson

Department of Chemistry, University of Maine, Orono, Maine 04469-5706, United States

Supporting Information

ABSTRACT: A series of metal−organic networks of CuSCN were prepared by direct reactions with substituted pyridine and aliphatic amine ligands, L. Thiocyanate bridging is seen in all but 1 of 11 new X-ray structures. Structures are reported for (CuSCN)L sheets (L = 3-chloro- and 3-bromopyridine, *N*-methylmorpholine), ladders (L = 2-ethylpyridine, *N*-methylpiperidine), and chains (L = 2,4,6-collidine). X-ray structures of $(CuSCN)L_2$ are chains (L = 4-ethyl- and 4-*t*-butylpyridine, piperidine, and morpholine). A unique *N*-thiocyanato monomer structure, $(CuSCN)(3\text{-ethylpyridine})_3$, is also reported. In most cases, amine ligands are thermally released at temperatures <100 °C. Strong yellow-to-green luminescence at ambient temperature is observed for the substituted pyridine complexes. High solid state quantum efficiencies are seen for many of the CuSCN-L complexes. Microsecond phosphorescence lifetimes seen for CuSCN-L are in direct contrast to the nanosecond-lifetime emission of CuSCN. MLCT associated with pyridine π^* orbitals is proposed as the excitation mechanism.

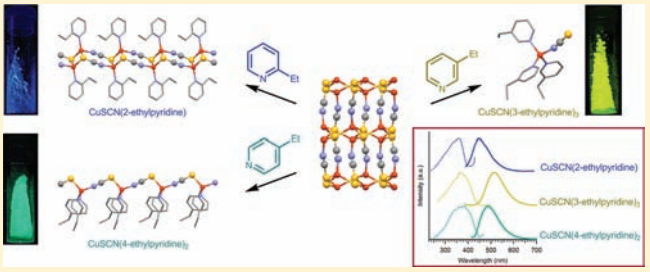

INTRODUCTION

In the course of our recent studies on the metal−organic network chemistry of copper(I) cyanide, we have noted that Cu(I) centers in CuCN chains are readily and reversibly decorated by amine and sulfide nucleophiles.[1,2] Coordination of nucleophiles shifts CuCN photoluminescence emission from the near UV (392 nm) into the visible region. As a result, the reversible luminescence-inducing reaction of amines with CuCN has potential use in sensing devices. In some cases, minor differences in the amine (e.g., between piperidine, *N*-methylpiperidine, and *N*-ethylpiperidine) result in remarkably different emission colors.[2] X-ray analysis of $CuCNL_n$ complexes confirmed the addition of amine or sulfide ligands to copper centers along the polymeric chains, increasing the Cu coordination number from 2- to 3- or 4-coordinate (Scheme 1A, L = amine or sulfide ligand, "□" = vacant coordination site).

Here we report the amine adduct chemistry of CuSCN. Both CuCN and CuSCN are air-stable Cu(I) species; however, the thiocyanate anion also stabilizes the Cu(II) oxidation state.[3] Copper(I) thiocyanate has attracted attention as a p-type semiconductor for solar applications.[4] Copper(I) thiocyanate differs structurally from CuCN because of the extensive bridging capabilities of sulfur. Three polymorphs of CuSCN are known,[5] each of which constitutes a 3D network containing 4-coordinate Cu and S (Scheme 1B). Coordination of amines or other nucleophiles would be expected to cause disruption of the CuSCN network. As suggested in Scheme 1B, addition of a single L per Cu would limit sulfur bridging, resulting in the formation of a 2D network, or perhaps a 1D ladder structure. Addition of two L per Cu would presumably lead to formation of simple decorated chains, like those seen for $CuCNL_n$.

To investigate the structural chemistry posited in Scheme 1B, we set out to identify the various structural types of CuSCN-amine compounds using the ligands shown in Chart 1, and also to examine product luminescence behavior. There have been many reports of the reaction of CuSCN with bidentate amines.[6] Chelating diamines form chains, and bridging diamines usually form sheets. Imidazolidine-2-thione and a thiazolidine-2-thione thiocarbonyl complexes of CuSCN have been reported.[7,8] Several complexes of CuSCN with simple amines were first noted in 1968.[9] However, no structural data were reported. Aside from a few reports of diamines behaving in monodentate fashion,[6f,g,10] only a single structural study of simple monodentate amine coordination to CuSCN has appeared.[11] In that paper the structures of 1:1 complexes (CuSCN)L (L = 2MePy and 26Lut), and 1:2 complexes $(CuSCN)L_2$ (L = 2MePy, 3MePy, 4MePy,[12] 24Lut, and Quin) were reported. No mention has yet been made of photoluminescence behavior by the CuSCN-monoamine complexes.

Received: April 20, 2011
Published: July 05, 2011

Scheme 1

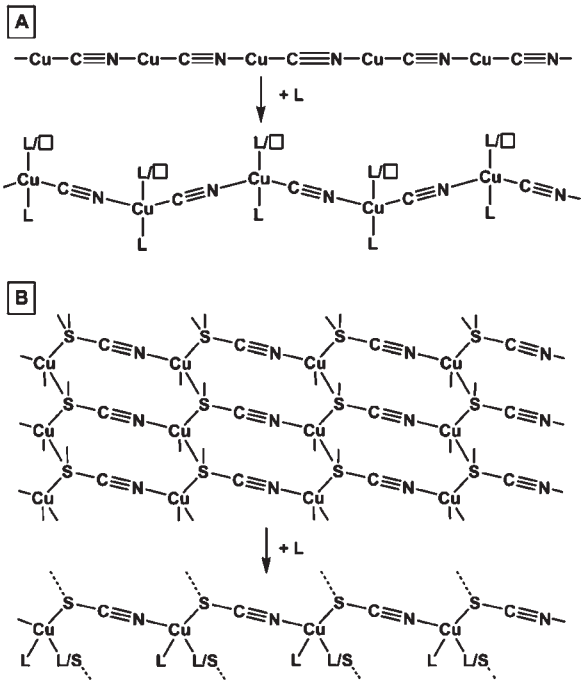

Chart 1

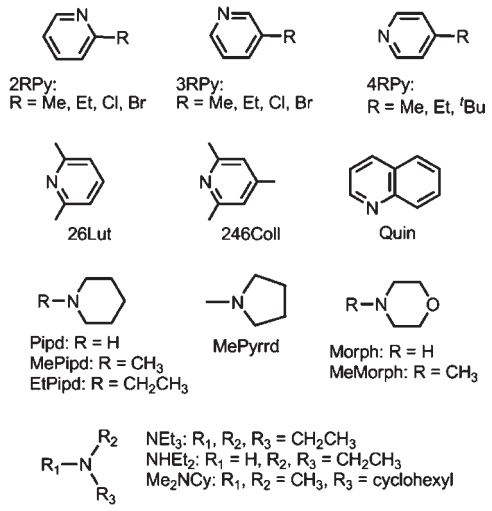

We considered it to be of interest to look for correlations in photophysical behavior between structurally related groups.

EXPERIMENTAL SECTION

Materials and Methods. All reagents were purchased from Aldrich or Acros and used without purification. Commercial CuSCN (Aldrich) was shown by FTIR to consist solely of the α-phase.[8] Analyses for C, H, and N were carried out by Atlantic Microlabs, Norcross, GA, or using a Thermo Scientific Flash 2000 Organic Elemental Analyzer with a Mettler Toledo XP6Microbalance. Steady-state photoluminescence spectra were recorded with a Model QuantaMaster-1046 photoluminescence spectrophotometer from Photon Technology International. The instrument is equipped with two excitation monochromators and a single emission monochromator with a 75 W xenon lamp. Low temperature steady-state photoluminescence measurements were achieved by using a Janis St-100 optical cryostat equipped with a Honeywell temperature controller. Liquid nitrogen was used as coolant. Lifetime measurements were conducted using an Opolette (HE) 355 II UV tunable laser with a range of 210−355 nm. The laser has a Nd:YAG flashlamp pumped with a pulse repetition rate of 20 Hz and an average output power 0.3 mW. The detection system is composed of a monochromator and photomultiplier from a Jobin Yvon Ramanor 2000 M Raman spectrometer. Data were collected by a Le Croy 9310C dual 400 MHz oscilloscope. The decays were averaged over 1000 sweeps and fitted using a curve fitting method in Igor Pro 6.0. Solid state quantum yields were measured on a Perkin-Elmer LS 55 spectrofluorimeter using a modified version of Mann's method,[13] in which sample comparison is made to a "perfect scatterer", Fluorilon FW-99 (Avian Technologies, Sunapee, NH). IR measurements were made on KBr pellets using a Digilab FTS 7000 FTIR spectrophotometer. Thermogravimetric analyses (TGA) were conducted using a TA Instruments Q500 in the dynamic (variable temp.) mode with a maximum heating rate of 50 °C/min to 300 °C under 60 mL/min. N_2 flow. The theoretical structure and energy of electronic states of aromatic amines were determined with Gaussian '03 software (Gaussian Inc.).[14] Density functional theory (DFT) optimization calculations were performed with the B3LYP functional[15] and 6-31+g* basis set as implemented in the software. These calculations were performed on the University of Maine supercomputer.

Syntheses. *CuSCN(2MePy)$_2$,* ***1a***. While stirring, 5 mL of 2MePy were added to solid CuSCN (0.182 g, 1.50 mmol), and the resulting suspension was sealed in a vial under Ar and stirred at ambient temperature for 4 d. The suspended solid was collected by means of filtration, washed with diethyl ether, and then air-dried. An off-white powder was isolated (0.409 g, 1.33 mmol, 88.6%). IR (KBr pellet, cm^{-1}) 2112, 801, 761, 727. Ligand loss was too rapid to allow for CHN analysis. TGA Calcd for CuSCN(2MePy): 69.8. Found: 68.6 (25−45 °C). Calcd for CuSCN: 39.5. Found: 37.7 (60−95 °C).

CuSCN(2MePy), ***1b***. Product **1a** was placed under vacuum overnight, producing an off-white powder (0.220 g, 1.02 mmol, 68.3%). IR (KBr pellet, cm^{-1}) 2112, 800, 761, 727 Anal. Calcd for $C_7H_7N_2CuS$: C, 39.15; H, 3.29; N, 13.04. Found: C, 41.12; H, 3.06; N, 12.78. TGA Calcd for CuSCN: 56.6. Found: 58.7 (55−90 °C).

CuSCN(3MePy)$_2$, ***2***. The procedure was identical to that used for **1a** using 3MePy. A yellow powder was isolated (0.376 g, 1.22 mmol, 81.4%). IR (KBr pellet, cm^{-1}) 2197, 796, 763, 703. Anal. Calcd for $C_{13}H_{14}N_3CuS$: C, 50.72; H, 4.58; N, 13.65. Found: C, 51.41; H, 4.67; N, 13.67. TGA Calcd for CuSCN(3MePy): 69.8. Found: 67.1 (50−75 °C). Calcd for CuSCN: 39.5. Found: 41.9 (75−105 °C).

CuSCN(4MePy)$_2$, ***3***. The procedure was identical to that used for **1a** using 4MePy. A tan powder was isolated (87.4%). IR (KBr pellet, cm^{-1}) 2122, 2096, 801, 768, 721. Anal. Calcd for $C_{13}H_{14}N_3CuS$: C, 50.72; H, 4.58; N, 13.65. Found: C, 52.86; H, 4.56; N, 13.48. TGA Calcd for CuSCN(4MePy): 69.8. Found: 69.2 (60−85 °C). Calcd for CuSCN: 39.5. Found: 40.4 (85−110 °C).

CuSCN(2EtPy), ***4***. The procedure was identical to that used for **1a** using 2EtPy. A beige powder was isolated (92.7%). IR (KBr pellet, cm^{-1}) 2163, 2104, 800, 752. Anal. Calcd for $C_8H_9N_2CuS$: C, 42.00; H, 3.97; N, 12.24. Found: C, 42.00; H, 3.89; N, 12.12. TGA Calcd for CuSCN: 53.2. Found: 54.0 (65−85 °C).

CuSCN(3EtPy)$_3$, ***5***. The procedure was identical to that used for **1a** using 3EtPy. A pale green powder was isolated (73.9%). IR (KBr pellet, cm^{-1}) 2114, 2082, 809, 748, 708. Anal. Calcd for $C_{22}H_{27}N_4CuS$: C, 59.64; H, 6.14; N, 12.64. Found: C, 58.96; H, 5.49; N, 12.36. TGA Calcd for CuSCN: 27.4. Found: 25.3 (40−160 °C).

CuSCN(4EtPy)$_2$, ***6***. The procedure was similar to that used for **1a** using 4EtPy. A dark colored solution resulted. Diethyl ether was layered onto the solution under Ar, resulting in precipitation of a yellow powder overnight

dx.doi.org/10.1021/ic200821f |*Inorg. Chem.* 2011, 50, 7239–7249

(88.1%). IR (KBr pellet, cm^{-1}) 2099, 2083, 826, 820, 783, 761. Anal. Calcd for $C_{15}H_{18}N_3CuS$: C, 53.63; H, 5.40; N, 12.51. Found: C, 53.63; H, 5.34; N, 12.43. TGA Calcd for CuSCN: 36.2. Found: 37.1 (65−85 °C).

CuSCN(Quin)$_2$, ***7***. The procedure was identical to that used for **1a** using Quin. A yellow powder was isolated (67.7%). IR (KBr pellet, cm^{-1}) 2096, 805, 781. Anal. Calcd for $C_{19}H_{14}N_3CuS$: C, 60.06; H, 3.71; N, 11.06. Found: C, 59.24; H, 3.58; N, 11.02. TGA Calcd for CuSCN(Quin): 66.0. Found: 65.8 (90−115 °C). Calcd for CuSCN: 32.0. Found: 32.6 (115−145 °C).

CuSCN(26Lut), ***8***. The procedure was identical to that used for **1a** using 26Lut. A white powder was isolated (62.1%). IR (KBr pellet, cm^{-1}) 2120, 779, 768. Anal. Calcd for $C_8H_9N_2CuS$: C, 42.00; H, 3.97; N, 12.24. Found: C, 42.43; H, 4.03; N, 12.43. TGA Calcd for CuSCN: 53.2. Found: 54.1 (70−105 °C).

CuSCN(246Coll), ***9***. The procedure was identical to that used for **1a** using 246Coll. A tan powder was isolated (93.2%). IR (KBr pellet, cm^{-1}) 2116, 851, 800. Anal. Calcd for $C_9H_{11}N_2CuS$: C, 44.52; H, 4.57; N, 11.54. Found: C, 42.80; H, 4.52; N, 11.39. TGA Calcd for CuSCN: 50.1. Found: 51.0 (75−110 °C).

CuSCN(4^{t}BuPy)$_2$, ***10***. The procedure was identical to that used for **1a** using 4^{t}BuPy. A pale green powder was isolated (86.9%). IR (KBr pellet, cm^{-1}) 2087, 829, 797. Anal. Calcd for $C_{19}H_{26}N_3CuS$: C, 58.21; H, 6.68; N, 10.72. Found: C, 56.61; H, 6.38; N, 10.47. TGA Calcd for CuSCN: 31.0. Found: 29.8 (70−230 °C).

CuSCN(3ClPy)$_2$, ***11a***. The procedure was identical to that used for **1a** using 3ClPy. A yellow powder was isolated (91.8%). IR (KBr pellet, cm^{-1}) 2118, 2100, 804, 766, 738, 694. Anal. Calcd for $C_{11}H_8N_3Cl_2CuS$: C, 37.89; H, 2.31; N, 12.05. Found: C, 37.40; H, 2.26; N, 11.99. TGA Calcd for $(CuSCN)_3(3ClPy)_2$: 56.5. Found: 59.8 (50−70 °C). Calcd for CuSCN: 34.9. Found: 35.5 (70−90 °C).

CuSCN(3BrPy)$_2$, ***12a***. The procedure was identical to that used for **1a** using 3BrPy. A yellow powder was isolated (60.6%). IR (KBr pellet, cm^{-1}) 2116, 2099, 802, 799, 763, 710, 693. Anal. Calcd for $C_{11}H_8N_3Br_2CuS$: C, 30.19; H, 1.84; N, 9.60. Found: C, 31.21; H, 1.93; N, 9.87. TGA Calcd for $(CuSCN)_3(3BrPy)_2$: 63.9. Found: 63.8 (60−80 °C). Calcd for CuSCN: 27.8. Found: 28.3 (80−110 °C).

CuSCN(Pipd)$_2$, ***13a***. The procedure was identical to that used for **1a** using Pipd. A tan powder was isolated (79.6%). IR (KBr pellet, cm^{-1}) 2167, 2111, 869, 847, 771, 757. Ligand loss was too rapid to allow for CHN analysis. TGA Calcd for CuSCN(Pipd): 76.4. Found: 74.9 (35−50 °C). Calcd for CuSCN: 44.9. Found: 44.2 (50−105 °C).

CuSCN(Pipd), ***13b***. Product **13a** was placed under vacuum line overnight, producing a white powder. IR (KBr pellet, cm^{-1}) 2113, 870, 847, 770. Anal. Calcd for $C_6H_{11}N_2CuS$: C, 34.85; H, 5.36; N, 13.55. Found: C, 35.81; H, 5.43; N, 15.60. TGA Calcd for CuSCN: 58.8. Found: 58.5 (60−105 °C).

CuSCN(MePipd), ***14***. The procedure was identical to that used for **1a** using MePipd. A yellow powder was isolated (83.6%). IR (KBr pellet, cm^{-1}) 2116, 2108, 860, 774, 753. Anal. Calcd for $C_7H_{13}N_2CuS$: C, 38.08; H, 5.93; N, 12.69. Found: C, 37.72; H, 5.92; N, 12.57. TGA Calcd for CuSCN: 55.1. Found: 56.1 (55−85 °C).

CuSCN(Morph)$_2$, ***15***. The procedure was identical to that used for **1a** using Morph. A white powder was isolated (92.8%). IR (KBr pellet, cm^{-1}) 2089, 863, 763, 623. Anal. Calcd for $C_9H_{18}N_3CuO_2S$: C, 36.54; H, 6.13; N, 14.20. Found: C, 36.49; H, 6.32; N, 14.13. CuSCN(Morph): 70.6. Found: 69.4 (35−95 °C). TGA Calcd for CuSCN: 41.1. Found: 41.4 (95−130 °C).

CuSCN(MeMorph), ***16***. The procedure was identical to that used for **1a** using MeMorph. A white powder was isolated (86.8%). IR (KBr pellet, cm^{-1}) 2174, 2118, 895, 864, 785, 758. Anal. Calcd for $C_6H_{11}N_2CuOS$: C, 32.35; H, 4.98; N, 12.57. Found: C, 32.40; H, 4.62; N, 12.11. TGA Calcd for CuSCN: 54.6. Found: 56.1 (60−95 °C).

CuSCN(MePyrrd), ***17***. The procedure was identical to that used for **1a** using MePyrrd. A white powder was isolated (89.3%). IR (KBr pellet, cm^{-1}) 2122, 870, 756. Anal. Calcd for $C_6H_{11}N_2CuS$: C, 34.85; H, 5.36; N, 13.55. Found: C, 34.45; H, 5.36; N, 13.43. TGA Calcd for CuSCN: 58.8. Found: 60.5 (55−75 °C).

CuSCN(NHEt$_2$), ***18***. The procedure was identical to that used for **1a** using $NHEt_2$. A pale green powder was isolated (83.8%). IR (KBr pellet, cm^{-1}) 2173, 2111, 2097, 820, 791, 766. Anal. Calcd for $C_5H_{11}N_2CuS$: C, 30.84; H, 5.69; N, 14.38. Found: C, 26.77; H, 5.00; N, 14.50. TGA Calcd for CuSCN: 62.4. Found: 64.4 (35−60 °C).

$(CuSCN)_3(NMe_2Cy)_2$, ***19***. The procedure was identical to that used for **1a** using NMe_2Cy. A beige powder was isolated (97.5%). IR (KBr pellet, cm^{-1}) 2114, 894, 858, 835, 777, 750. Anal. Calcd for $C_{19}H_{34}N_5Cu_3S_3$: C, 36.85; H, 5.53; N, 11.31. Found: C, 37.60; H, 5.40; N, 10.82. TGA Calcd for CuSCN: 58.9. Found: 57.3 (60−80 °C).

X-ray Analysis. Single crystal determinations were carried out using a Bruker SMART Apex II diffractometer using graphite-monochromated Cu Kα radiation.[16] The data were corrected for Lorentz and polarization[17] effects and absorption using SADABS.[18] The structures were solved by use of direct methods or Patterson map. Least squares refinement on F^2 was used for all reflections. Structure solution, refinement, and the calculation of derived results were performed using the SHELXTL[19] package of software. The non-hydrogen atoms were refined anisotropically. In all cases, hydrogen atoms were located, then placed in theoretical positions.

Powder diffraction analysis was carried out on the instrument described above. Samples were ground and prepared as mulls using Paratone N oil. Four 180 s frames were collected, covering 8−100° 2θ. Frames were merged using the SMART Apex II software[16] and were further processed using DIFFRAC-Plus and EVA software.[20] Simulated powder patterns from single crystal determinations were generated using the Crystallographica program.[21] Experimental and calculated powder diffraction results are provided in the Supporting Information.

RESULTS AND DISCUSSION

Synthesis. Amine (L) adduct powders were easily prepared by stirring the solid CuSCN suspended in neat liquid amine. In the absence of heating, a period of several days was required for complete conversion. Alternatively, when the neat mixture was heated to 70 °C in a sealed tube, the reactions proceeded more rapidly (usually being completed in one night) and often produced X-ray quality crystals. (The CuCN-L products reported in our previous contributions[2] can also be made via the ambient temperature technique, as well as by the previously reported heated tube syntheses.) Only in the case of 4EtPy did the CuSCN dissolve in the amine at ambient temperature. (Interestingly, identical behavior was noted for CuCN in 4EtPy.) In this case the product (**6**) was coaxed from solution by layering the mixture with diethyl ether under inert atmosphere. The use of L = EtPipd, NEt_3, 2ClPy and 2BrPy returned unreacted CuSCN at both temperatures. All products except **5**, **1a** and **13a** (as described below) showed indefinite stability. Except as noted, the discussions below center around compounds formed at ambient temperature since complete reactions and homogeneous products were the rule under these conditions.

The stoichiometry of the CuSCN-L products was readily determined via thermogravimetric analysis (TGA), as previously noted for CuCN-L products.[2] Analytical TGA data are listed in the Experimental Section. In all cases, except for that of the molecular 3EtPy complex (**5**), heating of solid CuSCN-L sample to 300 °C afforded clean recovery of CuSCN, allowing for ready identification of CuSCN:L ratio. Stoichiometries were further

dx.doi.org/10.1021/ic200821f |*Inorg. Chem.* 2011, 50, 7239–7249

Table 1. Synthetic and Structural Summary

ligand[a]	product[b]	CuSCN/L	structure type	SCN bridging mode	Cu coordination no.
2MePy[c]	**1a**	1:2	**A**, helical chain[d]	S,N-bridged	4-coordinate
	1b	1:1	**B**, ladder[d]	S,S,N-bridged	4-coordinate
3MePy	**2**	1:2	**A**, planar zigzag chain[d]	S,N-bridged	4-coordinate
4MePy	**3**	1:2	**A**, planar zigzag chain[d]	S,N-bridged	4-coordinate
2EtPy	**4**	1:1	**B**, ladder	S,S,N-bridged	4-coordinate
3EtPy	**5**	1:3	**D**, monomer	N-bound	4-coordinate
4EtPy	**6**	1:2	**A**, planar zigzag chain	S,N-bridged	4-coordinate
Quin	**7**	1:2	**A**, helical chain[d]	S,N-bridged	4-coordinate
26Lut	**8**	1:1	**A′**, helical chain[d]	S,N-bridged	3-coordinate
246Coll	**9**	1:1	**A′**, planar zigzag chain	S,N-bridged	3-coordinate
4^{t}BuPy	**10**	1:2	**A**, helical chain	S,N-bridged	4-coordinate
3ClPy[e]	**11a**	1:2			
	11b	1:1	**C**, rippled sheet	S,S,N-bridged	4-coordinate
3BrPy[e]	**12a**	1:2			
	12b	1:1	**C**, rippled sheet	S,S,N-bridged	4-coordinate
Pipd[c]	**13a**	1:2	**A**, planar zigzag chain	S,N-bridged	4-coordinate
	13b	1:1			
MePipd	**14**	1:1	**B**, ladder	S,S,N-bridged	4-coordinate
Morph	**15**	1:2	**A**, planar zigzag chain	S,N-bridged	4-coordinate
MeMorph	**16**	1:1	**C**, rippled sheet	S,S,N-bridged	4-coordinate
MePyrrd	**17**	1:1			
$NHEt_2$	**18**	1:1			
NMe_2Cy	**19**	3:2			

[a] No reaction with EtPipd, NEt_3, 2ClPy, 2BrPy. [b] Products prepared at 25 °C, except as noted. [c] 1:2 Product formed initially, converting to 1:1 product under vacuum. [d] Reference 11. [e] 1:2 Product formed at 25 °C and 1:1 product formed at 70 °C.

confirmed by elemental analysis. The CuSCN/L ratios found were 1:1, 3:2, 1:2, and 1:3, see Table 1. Single phases were formed in most cases and product identities were further confirmed by comparison of powder X-ray diffraction (PXRD) data to PXRD patterns calculated from authentic crystal structures (see Supporting Information).

Among the amines investigated, three gave evidence of mixed stoichiometry products: 2MePy, Pipd, and MeMorph. The initial CuSCN-2MePy and CuSCN-Pipd products were identified using TGA as being $(CuSCN)L_2$ (1:2) compounds, **1a** and **13a**. However, L loss began immediately, making CHN analysis impossible. Ligand loss ultimately resulted in 1:1 products **1b** and **13b**, as confirmed by CHN analysis. X-ray structures for both 1:2 and 1:1 CuSCN complexes of 2MePy are known.[11] PXRD of the 1:2 2MePy product **1a** produced here did not match the calculated pattern from reported compound $CuSCN(2MePy)_2$, but **1b** did match the reported CuSCN(2MePy) pattern (Figures S1 and S2, Supporting Information). The PXRD of **13a** matched the calculated pattern for the $CuSCN(Pipd)_2$ (Figure S14, Supporting Information). For the CuSCN-MeMorph product, both TGA and CHN indicated pure CuSCN(MeMorph), **16**. However, PXRD indicated the presence of a minor component (Figure S17, Supporting Information). Given the good quality analytical data, this impurity is probably a polymorph. In all other cases single products were found. The rapid progression of 2MePy loss during the conversion: **1a** (yellow emission) → **1b** (blue emission) is shown as a series of photos under 365 nm excitation in Figure S56 (Supporting Information).

The heated tube reaction products were usually found to be identical to those made at ambient temperature, although NMe_2Cy failed to react with CuSCN under heating. For L = 26Lut, 246Coll, and MePipd, PXRD and TGA showed evidence of unreacted CuSCN in heated reactions. Crystals isolated from these 70 °C reactions produced structures in agreement with ambient temperature PXRD results. On the other hand, the 3ClPy and 3BrPy heated reactions gave products showing 1:1 stoichiometry by TGA and yielded 1:1 X-ray structures. These results were in sharp contrast to the 1:2 ambient temperature products obtained with 3ClPy and 3BrPy.

X-ray Structures. Eleven new X-ray structures emerged from the current study. Refinement details for all structures are summarized in Table 2, and selected bond lengths and angles are given in Table 3. Among the CuSCN-L structures now known,[6,7,10,11] several structural themes can be identified (see Chart 2). As was predicted in Scheme 1, coordination of two L per Cu invariably produces a polymer (**A** in Chart 2). Coordination of a single L per Cu can lead to any of three outcomes: polymer **A′** (□ = vacant coordination site), ladder (double chain) **B**, or sheet network **C**. While polymers **A** and **A′** feature simple S,N-bridged thiocyanate, in networks **B** and **C** thiocyanate bridging is expanded to S,S,N-type. New to this study is molecular structure **D**, which features terminal N-bonded thiocyanate. As shown in Table 3, the Cu−S−C, S−C−N, and C−N−Cu bond angles were 95.15(7)−110.76(7)°, 177.7(4)−179.39(19)°, and 156.3(3)−175.62(14)°, suggesting that the S−C≡N thiocyanate resonance form dominates over S=C=N. Copper−amine bond lengths appear to be slightly shorter for **A′** (1.9479(19), 1.993(3) Å) than for **A** (2.043(5)−2.1376(11) Å), **B** (2.000(3)−2.0919(18) Å), **C** (2.012(2)−2.1279(12) Å), or **D** (2.0286(18), 2.0322(17), 2.0420(16) Å).

dx.doi.org/10.1021/ic200821f |*Inorg. Chem.* 2011, 50, 7239–7249

Table 2. Crystal and Structure Refinement Data

	4	5	6	9	10	11b
CCDC deposit no.	808077	808078	808082	808079	808084	808083
color and habit	colorless prism	yellow prism	yellow block	colorless prism	yellow plate	yellow plate
size, mm	0.22 × 0.10 × 0.09	0.44 × 0.10 × 0.09	0.37 × 0.23 × 0.20	0.24 × 0.06 × 0.05	0.41 × 0.39 × 0.10	0.38 × 0.36 × 0.08
formula	$C_8H_9CuN_2S$	$C_{22}H_{27}CuN_4S$	$C_{15}H_{18}CuN_3S$	$C_9H_{11}CuN_2S$	$C_{19}H_{26}CuN_3S$	$C_6H_4ClCuN_2S$
formula weight	228.77	443.08	335.92	242.80	392.03	235.16
space group	$P2_1/c$ (#14)	$P2_1$ (#4)	$P2_1/n$ (#14)	$P2_1/c$ (#14)	$P2_1/c$ (#14)	$P2_1/n$ (#14)
a, Å	5.8113(2)	8.68570(10)	15.3390(2)	5.6098(3)	12.6385(2)	3.78140(10)
b, Å	15.4887(6)	14.6171(3)	5.85820(10)	13.2503(8)	10.6785(2)	24.2829(8)
c, Å	9.7322(4)	9.4291(2)	18.4560(2)	14.2590(9)	15.1085(2)	8.3855(3)
β, deg	91.121(2)	111.9520(10)	112.7990(3)	91.884(4)	102.9720(10)	91.0050(10)
volume, Å^3	875.82(6)	1110.32(4)	1528.86(2)	1059.32(11)	1987.01(6)	769.87(4)
Z	4	2	4	4	4	4
ρ_{calc}, g cm^{-3}	1.735	1.325	1.459	1.522	1.310	2.029
F_{000}	464	464	696	496	824	464
μ(Cu Kα), mm^{-1}	5.257	2.365	3.223	4.381	2.553	9.128
temperature, K	100	100	100	100	100	100
residuals:[a] R; R_w	0.0516; 0.1423	0.0210; 0.0522	0.0246; 0.0656	0.0243; 0.0629	0.0228; 0.0655	0.0282; 0.0843
goodness of fit	1.218	1.025	1.057	1.067	1.002	1.040

	12b	13a	14	15	16
CCDC deposit no.	808080	808085	808081	816484	808086
color and habit	colorless plate	colorless plate	colorless blade	colorless blade	colorless plate
size, mm	0.18 × 0.12 × 0.03	0.33 × 0.19 × 0.02	0.26 × 0.11 × 0.05	0.36 × 0.09 × 0.03	0.21 × 0.19 × 0.07
formula	$C_6H_4BrCuN_2S$	$C_{11}H_{22}CuN_3S$	$C_{14}H_{26}Cu_2N_4S_2$	$C_9H_{18}CuN_3O_2S$	$C_6H_{11}CuN_2OS$
formula weight	279.62	291.92	441.59	295.86	222.77
space group	$P2_1/n$ (#14)	*Pnma* (#62)	$P2_1/c$ (#14)	*Pnma* (#62)	*Pbca* (#61)
a, Å	3.8166(3)	10.9672(4)	11.7388(3)	11.5188(10)	6.81330(10)
b, Å	24.2881(16)	21.4419(8)	13.0673(3)	17.8699(6)	10.6817(2)
c, Å	8.4924(6)	5.8806(2)	12.6949(3)	5.6997(2)	23.2105(4)
β, deg	91.714(4)	90	112.1240(10)	90	90
volume, Å^3	786.88(10)	1382.87(9)	1803.95(8)	1173.23(7)	1689.21(5)
Z	4	4	4	4	8
ρ_{calc}, g cm^{-3}	2.360	1.402	1.626	1.675	1.752
F_{000}	536	616	9112	616	912
temperature, K	100	100	100	100	100
residuals:[a] R; R_w	0.0287; 0.0745	0.0358; 0.0984	0.0250; 0.0623	0.0200; 0.0562	0.0180; 0.0521
goodness of fit	1.091	1.082	1.034	1.075	1.005

[a] $R = R_1 = \Sigma||F_o| - |F_c||/\Sigma|F_o|$ for observed data only. $R_w = wR_2 = \{\Sigma w(F_o^2 - F_c^2)^2/\Sigma w(F_o^2)^2\}^{1/2}$ for all data.

The thiocyanate-S,N-bridged chain-type structure, **A**/**A**′, appears to be the most commonly encountered. Among these products two distinctions can be made: (1) $(CuSCN)L_2$ (1:2, **A**) vs (CuSCN)L (1:1, **A**′) and (2) zigzag vs helical chain type. In addition to the known **A**/**A**′ complexes **1a** (**A**, helical), **2** (**A**, zigzag), **3** (**A**, zigzag), **7** (**A**, helical), **8** (**A**′, helical), and $(CuSCN)(24Lut)_2$ (**A**, zigzag),[11] new **A**/**A**′ compounds include **6** (**A**, zigzag), **9** (**A**′, helical), **10** (**A**, helical), **13a** (**A**, zigzag), and **15** (**A**, zigzag). Type **A**/**A**′ also occurs for monodentate L = 2-cyanopyrazine and 4-hydroxypyrazine (both **A**, zigzag).[6f] Chain drawings of the new complexes are shown in Figure 1. It will be noted that the Pipd ligand in **13a** is bound to Cu in equatorial fashion, while Morph in **15** is bound axially, as are N-substituted amines MePipd and MeMorph in complexes **14** and **16** (see below). In contrast to the behavior in $CuCN(MeMorph)$,[2] no Cu···O interactions were seen for either **15** or **16** in the present study. In all 1:2 type **A** cases, bond angles around Cu were within ±10° of tetrahedral.

Formation of the 1:1 type **A**′ complexes was observed only for 26Lut and 246Coll, (and not for 24Lut[11]). Substitution of the crowded 2,6-aromatic positions seems to be required to exclude a second L from the chain. The two examples of type **A**′ (**8** and **9**) show a remarkable structural distinction. While 26Lut complex **8** features Cu bond angles within ±3° of trigonal,[11] the N_{amine}−Cu−NCS angle in 246Coll complex, **9**, measures 150.51(8)°. This angle makes the ring centroid−NCS distance roughly 3.4 Å, suggesting a $\pi-\pi$ interaction.

Ladder structure **B** has previously been noted for **1b** and (CuSCN)L (monodentate L = 1-ethyl-2-methylpyrazine and 1,7-phenanthroline).[6g,10a,11] New complexes **4** and **14** share this arrangement (see Figure 2). As is typical of the rhomboid Cu_2S_2 core, Cu−S−Cu angles are quite acute (<80°) in all five cases.

dx.doi.org/10.1021/ic200821f |*Inorg. Chem.* 2011, 50, 7239–7249

Table 3. Selected Bond Lengths and Angles for All Complexes[a]

		Complex **4**, (CuSCN)(2EtPy)[b,c]	
Cu−S	2.3380(15), 2.4865(14)	Cu−S−C	98.22(17), 106.10(18)
S−C	1.668(5)	S−C−N	179.0(5)
C−N	1.151(7)	C−N−Cu	159.6(4)
$Cu-N_{CS}$	1.991(5)	$S-Cu-N_{CS}$	101.28(13), 103.17(14)
$Cu-N_{am}$	2.026(5)	$N_{am}-Cu-N_{CS}$	109.5(2)
Cu···Cu	2.7701(15)	$S-Cu-N_{am}$	108.56(14), 122.23(14)
		S−Cu−S	109.99(5)
		Cu−S−Cu	70.01(5)
		Complex **5**, $(CuSCN)(3EtPy)_3$[b,d]	
S−C	1.642(2)	S−C−N	179.39(19)
C−N	2.049(7)-2.144(4)	C−N−Cu	163.12(18)
$Cu-N_{CS}$	2.028(2)	$N_{am}-Cu-N_{CS}$	102.05(8), 105.20(7), 105.36(7)
$Cu-N_{am}$	2.0286(18), 2.0322(17), 2.0420(16)	$N_{am}-Cu-N_{am}$	111.54(7), 114.69(6), 116.37(7)
		$S-Cu-N_{am}$	108.56(14), 122.23(14)
		Complex **6**, $(CuSCN)(4EtPy)_2$[b,e]	
Cu−S	2.123(4)	Cu−S−C	103.77(5)
S−C	1.6558(16)	S−C−N	179.22(17)
C−N	1.160(2)	C−N−Cu	173.29(14)
$Cu-N_{CS}$	1.9440(14)	$S-Cu-N_{CS}$	111.10(4)
$Cu-N_{am}$	2.0833(13), 2.0873(13)	$N_{am}-Cu-N_{CS}$	111.65(6), 113.33(6)
		$N_{am}-Cu-N_{am}$	99.19(5)
		$S-Cu-N_{am}$	110.25 (4), 110.77(4)
		Complex **9**, (CuSCN)(Coll)[e,f]	
Cu−S	2.3949(7)	Cu−S−C	97.13(8)
S−C	1.649(2)	S−C−N	179.0(2)
C−N	1.155(3)	C−N−Cu	170.23(19)
$Cu-N_{CS}$	1.868(2)	$S-Cu-N_{CS}$	105.50(6)
$Cu-N_{am}$	1.9479(19)	$N_{am}-Cu-N_{CS}$	150.51(8)
		$S-Cu-N_{am}$	103.99(6)
		Complex **10**, $(CuSCN)(4^tBuPy)_2$[b,e]	
Cu−S	2.3131(4)	Cu−S−C	98.76(5)
S−C	1.6580(14)	S−C−N	178.59(12)
C−N	1.1571(19)	C−N−Cu	176.72(12)
$Cu-N_{CS}$	1.9390(12)	$S-Cu-N_{CS}$	117.30(4)
$Cu-N_{am}$	2.0613(11), 2.1083(11)	$N_{am}-Cu-N_{CS}$	110.00(5), 110.55(5)
		$N_{am}-Cu-N_{am}$	101.24(4)
		$S-Cu-N_{am}$	104.21(3), 112.20(3)
		Complex **11b**, (CuSCN)(3ClPy)[b,c]	
Cu−S	2.3310(7), 2.3553(6)	Cu−S−C	102.29(8), 103.58(9)
S−C	1.670(3)	S−C−N	178.7(2)
C−N	1.153(3)	C−N−Cu	158.19(19)
$Cu-N_{CS}$	1.974(2)	$S-Cu-N_{CS}$	116.82(7), 117.18(7)
$Cu-N_{am}$	2.064(2)	$N_{am}-Cu-N_{CS}$	102.92(8)
		S−Cu−S	107.59(3)
		Cu−S−Cu	107.59(3)
		$S-Cu-N_{am}$	102.02(6), 108.88(6)
		Complex **12b**, (CuSCN)(3BrPy)[b,c]	
Cu−S	2.3376(10), 2.3585(9)	Cu−S−C	102.34(12), 104.84(12)
S−C	1.677(4)	S−C−N	178.8(3)
C−N	1.152(5)	C−N−Cu	156.3(3)
$Cu-N_{CS}$	1.974(3)	$S-Cu-N_{CS}$	116.21(9), 117.51(9)
$Cu-N_{am}$	2.065(3)	$N_{am}-Cu-N_{CS}$	102.10(12)

dx.doi.org/10.1021/ic200821f |*Inorg. Chem.* 2011, 50, 7239–7249

Table 3. Continued

		S−Cu−S	108.73(4)
		Cu−S−Cu	108.72(4)
		S−Cu−N_{am}	102.05(8), 108.68(8)
		Complex **13a**, $(CuSCN)(Pipd)_2$[b,e]	
Cu−S	2.3066(11)	Cu−S−C	103.69(14)
S−C	1.657(4)	S−C−N	177.7(4)
C−N	1.155(5)	C−N−Cu	172.8(3)
Cu−N_{CS}	1.941(4)	S−Cu−N_{CS}	113.15(11)
Cu−N_{am}	2.127(2)	N_{am}−Cu−N_{CS}	108.71(7)
		N_{am}−Cu−N_{am}	100.66(12)
		S−Cu−N_{am}	108.71(7)
		Complex **14**, $(CuSCN)(MePipd)$[b,c]	
Cu−S	2.3232(6), 2.4074(6), 2.4048(6), 2.5934(6)	Cu−S−C	96.52(7), 97.28(7), 104.98(7), 110.76(7)
S−C	1.659(2), 1.663(2)	S−C−N	178.60(19), 179.2(2)
C−N	1.162(3), 1.163(3)	C−N−Cu	159.52(17), 164.53(17)
Cu−N_{CS}	1.9467(18), 1.9719(18)	S−Cu−N_{CS}	97.29(5), 100.79(5), 102.34(5), 110.25(5)
Cu−N_{am}	2.0867(17), 2.0919(18)	N_{am}−Cu−N_{CS}	116.22(7), 123.26(7)
Cu···Cu	2.7009(6), *ca.* 3.08	S−Cu−N_{am}	102.68(5), 107.02(5), 116.03(5), 117.58(5)
		S−Cu−S	102.603(19), 111.717(17)
		Cu−S−Cu	68.284(17), 77.397(19)
		Complex **15**, $(CuSCN)(Morph)_2$[b,e]	
Cu−S	2.4410(6)	Cu−S−C	95.15(7)
S−C	1.657(2)	S−C−N	179.22(18)
C−N	1.163(3)	C−N−Cu	168.84(17)
Cu−N_{CS}	1.9399(18)	S−Cu−N_{CS}	107.10(5)
Cu−N_{am}	2.1376(11)	N_{am}−Cu−N_{CS}	121.13(4)
		N_{am}−Cu−N_{am}	100.14(6)
		S−Cu−N_{am}	102.21(3)
		Complex **16**, $(CuSCN)(MeMorph)$[b,c]	
Cu−S	2.3677(4), 2.3720(4)	Cu−S−C	101.38(6), 109.68(6)
S−C	1.6601(16)	S−C−N	177.85(15)
C−N	1.161(2)	C−N−Cu	175.62(14)
Cu−N_{CS}	1.9445(14)	S−Cu−N_{CS}	99.04(4), 110.22(4)
Cu−N_{am}	2.1279(12)	N_{am}−Cu−N_{CS}	121.08(5)
		S−Cu−N_{am}	105.70(4), 114.14(4)
		S−Cu−S	105.796(12)
		Cu−S−Cu	121.321(17)

[a] N_{am} and N_{CS} indicate amine and thiocyanate N atoms, respectively. [b] 4-Coordinate Cu atom. [c] S,S,N bridging SCN. [d] Terminal N-bound SCN. [e] S,N bridging SCN. [f] 3-Coordinate Cu atom.

This brings the copper atoms into relatively close proximity with one another; in some cases the Cu···Cu is slightly less than the sum of their van der Waals radii (ca. 2.8 Å).[22] Such is the case for the single Cu···Cu in **4** and for one of two Cu···Cu in **14**.

Putative opening of the Cu_2S_2 rings in ladder structure **B** produces an infinite sheet structure **C** similar to that reported for CuSCN complexes of monodentate 5-bromopyrimidine (5BrPym) and pyridazine (Pdz).[6g,10a] Isomorphic 3ClPy and 3BrPy complexes **11b** and **12b**, along with MeMorph complex **16**, are **C** sheets (see Figure 3). In **11b** and **12b** zigzag CuSCN chains are cross-linked by zigzag CuS linkages. The rippled sheet produces alternating inversion symmetry at the copper atoms, resulting in L decoration on both faces of the sheet. Complexes **11b** and **12b** are isostructural with CuSCN(Pdz). In contrast, all Cu−L units in CuSCN(5BrPym) point in the same direction. Complex **16** is structurally quite different that the other four **C** examples. In **16** both CuSCN and CuS chains form tightly coiled figure-8 helices. As with **11b** and **12b** and CuSCN(Pdz), the **16** sheet is decorated with L on both faces. Oxygen atoms in adjacent sheets point toward one another; there is a 2.5058(4) Å hydrogen-bond-like interaction between O1 and a hydrogen atom (H4A) on an adjacent L.

Interestingly, each of the three EtPy isomers resulted in a different CuSCN ratio and structural type. Thus, the 2EtPy and 4EtPy complexes (**4** and **6**) were of types **B** (1:1) and **A** (1:2), as described above. The 3EtPy complex (**5**) revealed a remarkable 1:3 stoichiometry, which was confirmed by the determination of the unique type **D** monomer structure. A simple tetrahedron, **5** reveals an N-coordinated thiocyanate ligand and three L ligands with roughly tetrahedral bond angles about Cu (102.05(8)−116.38(7)°). The shortest potential chain-forming Cu···S distance measures about 4.68 Å, confirming that this is a true monomer. Despite the relative softness of Cu(I), N-coordination of thiocyanate

dx.doi.org/10.1021/ic200821f |*Inorg. Chem.* 2011, 50, 7239–7249

Chart 2

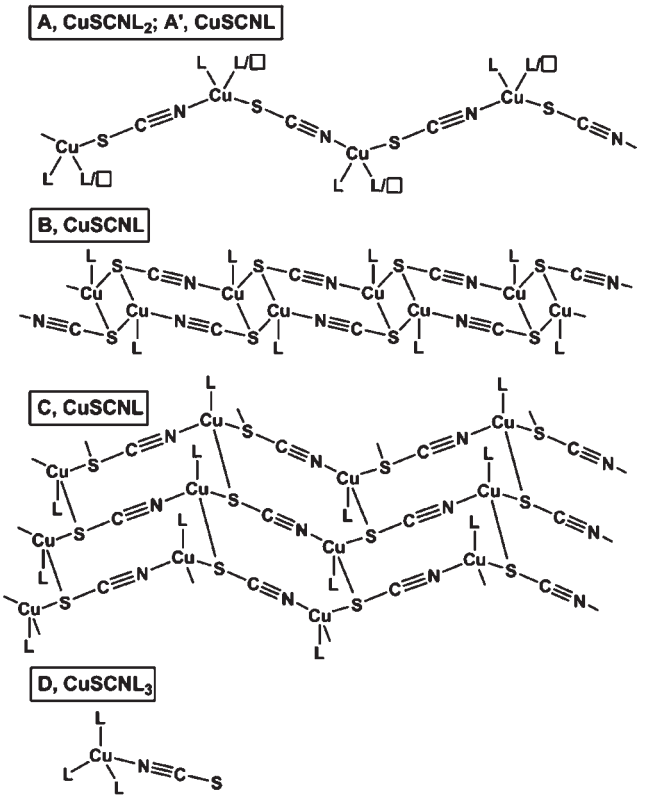

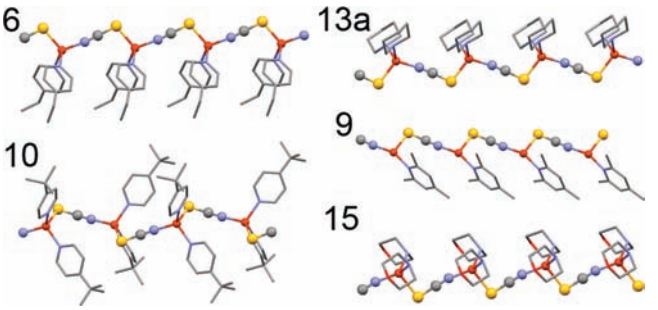

Figure 1. X-ray structures of **6**, **9**, **10**, **13a**, and **15**. Key to Figures 1−4: Copper and thiocyanate atoms shown as spheres. Amine ligands are shown as wireframe. Color scheme for all X-ray figures: orange = Cu, gray = C, blue = N, yellow = S, green = Cl, red = O. Hydrogen atoms omitted.

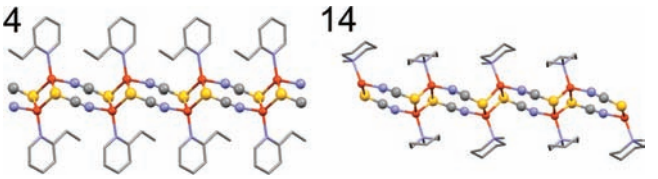

Figure 2. X-ray structures of **4** and **14**.

(as is seen for **5**) is in fact more common than S-coordination in related crystal structures.[3]

It has been claimed that reduced charge density on Cu and enhanced ligand σ-donation tend to favor S-coordinated thiocyanate

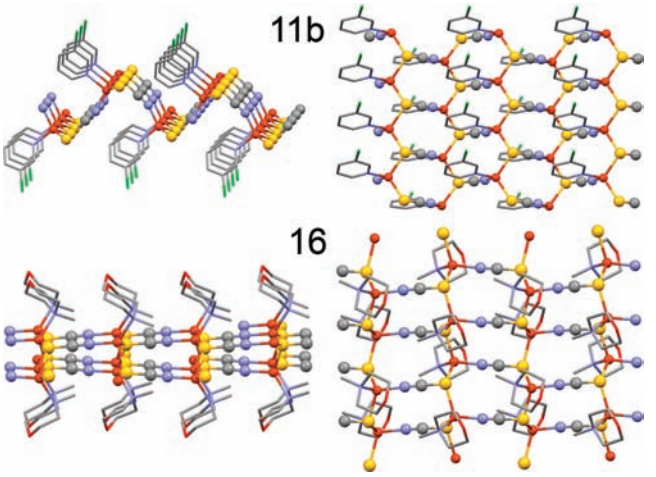

Figure 3. X-ray structures of **11b** (views along *a*- and *b*-axes) and **16** (views along *a*- and *c*-axes).

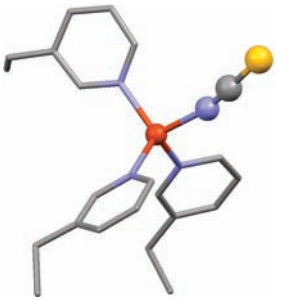

Figure 4. X-ray structure of **5**.

(including multiple S-bridging), while higher charge density on the metal and ligand π-acceptance favor N-attachment.[3] Based on this reasoning, the presence of three substituted pyridine ligands in **5** would lead one to expect an N-coordinated SCN, as is actually seen. The bridging SCN species in the present structural study lent no particular support to the above claims, which predict S,S,N-bridging for the σ-donor aliphatic amines and S,N-bridging for the π-acceptor pyridine ligands. For CuSCN-L structures, S,S,N-bridging is seen in 1:1 complexes incorporating both aromatic ligand complexes **1b**, **4**, **11b**, **12b** and aliphatic ligand complexes **14** and **16**. Thiocyanate S,N-bridging is also observed for both types of amines: **1a**, **2**, **3**, **6**−**10**, (aromatic ligands) and **13a** and **15** (aliphatic ligands). All of these complexes (except 1:1 **8** and **9**) are of 1:2 stoichiometry. Presumably, **8** and **9** are prevented from producing either 1:2 chains or 1:1 networks because of the demanding cone angles of 26Lut and 246Coll. Thus, the number of amine ligands coordinated appears to be a more significant factor than the donor/acceptor nature of the ligands in determining the mode of SCN bridging.

Thermal Analysis. Thermogravimetric analysis (TGA) of CuSCN-L networks revealed smooth loss of L, as seen previously for CuCN-L complexes.[1,2] Mass losses, temperature ranges, and interpretations for the bulk powder samples are provided in the Experimental Section; the TGA traces are included in the Supporting Information. For $(CuSCN)L_{>1}$ complexes stage-wise loss of ligand, for example, $(CuSCN)L_2 \rightarrow (CuSCN)L \rightarrow CuSCN$, was usually obvious. Decomposition temperatures were very modest,

dx.doi.org/10.1021/ic200821f |*Inorg. Chem.* 2011, 50, 7239–7249

Table 4. Luminescence Results

complex[a]	excitation λ_{max}, nm	emission λ_{max}, nm (color)	stokes shift, cm^{-1} [b]	lifetime, μs	quantum yield
1:2 3MePy, **2**	341	493 (yellow-green)	9042	9.1	0.31
1:2 4MePy, **3**	387	480 (blue-green)	5006	9.1	0.47
1:1 2EtPy, **4**	342	451 (blue)	7067	0.19	<0.03
1:3 3EtPy, **5**	367	513 (yellow-green)	7755	6.7	0.60
1:2 4EtPy, **6**	386	486 (yellow-green)	5331	1.9	0.04
1:2 Quin, **7**	358	585 (orange)	10840	0.59	<0.03
1:1 26Lut, **8**	337	434 (blue)	6633	4.9	0.34
1:1 246Coll, **9**	341	421 (blue)	5573	6.7	<0.03
1:2 4^tBuPy, **10**	367	521 (yellow-green)	8054	10.2	0.34
1:2 3ClPy, **11a**	360	524 (yellow)	8694	8.8	0.66
1:2 3BrPy, **12a**	367	529 (yellow)	8344	8.3	0.48

[a] Other isolated complexes showed no luminescence, except for **1b**, which shows yellow-green emission, but was not further studied. [b] Calculated between longest excitation λ_{max} and shortest emission λ_{max}.

usually starting well below 100 °C. For L = substituted pyridine ligands, CuSCN-L complexes initiated decomposition at temperatures consistently 20−30 °C lower than those of the corresponding CuCN-L complexes. Thus, it appears that binding of pyridine ligands to CuCN is slightly stronger than that to CuSCN. No consistent trend was apparent between the initial decomposition temperatures of CuSCN-L versus those of CuCN-L for aliphatic amines.

Infrared Spectroscopy. Solid state IR spectroscopy of CuSCN-L samples revealed the bands expected for metal thiocyanates in two regions: 2082−2197 (C≡N) and 693−895 (S−C) cm^{-1}. Terminal metal N-thiocyanate and S-thiocyanate bands are typically found near 2050 and 2100 cm^{-1}, respectively.[8] Bridging SCN bands are found above 2100 cm^{-1}. In the current study, all complexes except **5** are either confirmed or strongly suspected to contain bridging SCN. Accordingly, all these complexes showed C≡N bands no lower in frequency than 2082 cm^{-1}. However, complex **5**, which has been confirmed to contain an N-bonded terminal thiocyanate, produced bands at 2114 and 2082 cm^{-1}, which would be more consistent with S-bonding or bridging behavior. Although the lower frequency band can be used to interpret the bonding mode of thiocyanate,[8,23] complications are introduced by the presence of aromatic ligand modes in the same region.

Luminescence Spectroscopy. Unlike solid CuCN, CuSCN itself shows only very weak luminescence. The peak excitation for CuSCN is found at short wavelength in the vicinity of 250 nm with a broad emission band centered at 400 nm (see Figure 5). This large Stokes shift of 16,300 cm^{-1} is suggestive of significant electronic configuration change, while the weak emission intensity is due to a nonradiative deactivation pathway. We have previously reported that luminescence behavior in CuCN is the result of excitation between π orbitals, specifically between the d_{Cu}/π_{CN} highest occupied molecular orbital (HOMO) and the p_{Cu}/π^*_{CN} lowest unoccupied molecular orbital (LUMO).[24] However, this is not the case for CuSCN. The reflectance results for pure CuSCN powder show broad absorption from 240 to 330 nm, which is due to the presence of copper metal centered transition (MC) and metal-to-ligand-charge-transfer (MLCT). According to the excitation spectrum, the higher energy MC transition, for example, $d^{10}\rightarrow d^9s^1$ or $d^{10}\rightarrow d^9p^1$, is responsible for the weak emission at 400 nm. In the excited state, the copper metal center becomes d^9, and the electronic configuration change leads to the observed large Stokes shift. Also the short luminescence lifetime (16 ns) for CuSCN indicates that this transition is spin allowed. As a ligand for Cu(I), thiocyanate is a poorer acceptor for MLCT compared to cyanide.

With the addition of substituted pyridines, the solid state photophysical properties of the CuSCN-L compounds change dramatically, producing long lifetimes (μs) and usually intense emission. Luminescence results for the photoactive compounds are collected in Table 4. Additional spectra are included in the Supporting Information. The 2MePy complexes were not studied because of their tendency to lose ligand. Each of the luminescent CuSCN-L complexes showed a very broad excitation band occurring between 341 and 387 nm. Some fine structure is evident in these bands. The longer excitation wavelength for CuSCN-L compared to that of CuSCN suggests that less disruption of the network occurs during excitation, presumably since ligand addition has already broken up the 3D CuSCN lattice. The CuSCN-L complexes generally show emission bands in the green-to-yellow region. However, the 26Lut and 246Coll complexes **8** and **9** show exceptional behavior with relatively short excitation (ca. 340 nm) and emission (ca. 425 nm) wavelengths. Similar observations were also noted for the ladder-structure complex **4**. Species **4**, **8**, and **9** are the only complexes reported herein that show blue emission. Emission lifetime and quantum yield data were measured. In all cases lifetime curves were easily fit to single exponential decays with values in the microsecond range. This suggests phosphorescent behavior, consistent with previous studies on copper(I) complexes.[6h,25] Solid state quantum yields are quite high (0.31−0.66) for complexes **2**, **3**, **5**, **8**, **10**, **11a**, and **12a**.

For most Cu(I) compounds, the long-lived emission usually originates from MLCT transitions.[26] We have found that no CuSCN-L complex of aliphatic amines shows luminescent behavior. The apparent requirement of ligand aromaticity for visible emission indicates an MLCT transition, in which the empty π^* orbitals of amines accept electrons from copper. The excitation peak shapes of all pyridine-based complexes are similar (Supporting Information). However, the 26Lut and 246Coll complexes **8** and **9**, and the 2EtPy complex **4** exhibit short excitation wavelength, as shown in Figure 5. Also interesting is the fact that **4**, **8**, and **9** have the highest energy emission peaks (451, 434, and 421 nm, see Table 4) and Quin complex **7** has the lowest (585 nm). The pyridine-based complexes show intermediate emission energies (ranging from 480 to 530 nm). Our density functional theory (DFT) calculations show that the energy order of the LUMO for these organic ligands is 26Lut (−94.75 kJ/mol) > pyridine

dx.doi.org/10.1021/ic200821f |*Inorg. Chem.* 2011, 50, 7239–7249

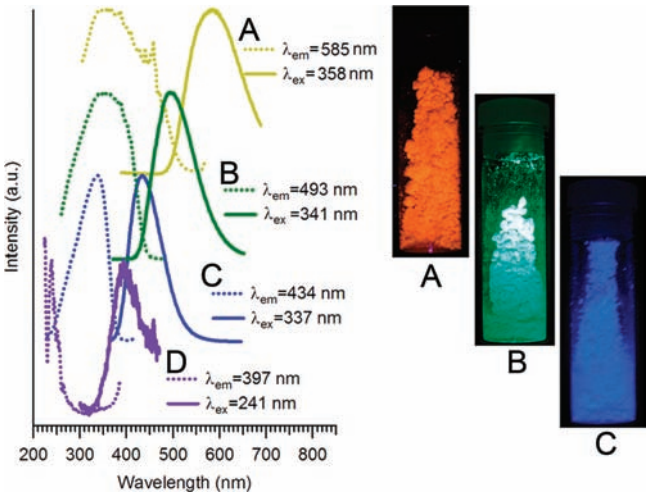

Figure 5. Luminescence spectra at 298 K and luminescence photographs under 365 nm light of (A) $(CuSCN)(Quin)_2$, **7**, (B) $(CuSCN)(3MePy)_2$, **2**, (C) (CuSCN)(26Lut), **8**. (D) Luminescence spectra of pure CuSCN powder at 298 K.

(−119.49 kJ/mol) > Quin (−180.71 kJ/mol). (The full table of DFT results may be found in Table S1 in the Supporting Information.) The extra conjugation provides further stabilization while the methyl groups weaken the aromaticity. This result can be used to understand the MLCT transition, in which aromatic amines provide empty π^* orbitals as the LUMO. The Quin complex **7** has the smallest HOMO−LUMO gap and gives an orange color; the 26Lut and 246Coll complexes **8** and **9** have the large band gaps and exhibit blue emission. For pyridine-based complexes, the energy differences between HOMO and LUMO are intermediate and produce yellow to yellow-green color, depending on the groups on the aromatic ring. Presumably, the higher energy emission seen in ladder complex **4** is associated with a MC transition. It is noteworthy that this species shows the shortest lifetime of any CuSCN-L.

Lowering of the LUMO symmetry through bending of the polymer chain at copper appears to be responsible for bathochromic emission shifts upon ligand addition. The situation is probably similar to that of CuCN, which also shows unsaturation along the chain. However, there are two very significant behavioral differences between CuCN-L and CuSCN-L: (1) aliphatic amines produce luminescent complexes of CuCN, but not CuSCN, and (2) the CuSCN-L complexes reported herein lack both the additional low energy band and the thermochromic behavior noted for many CuCN-L species. This may be because CN is a better acceptor for MLCT than is SCN. There are two emissive pathways for CuCN-L compounds (Cu to CN and Cu to L) while only one radiative deactivation pathway for CuSCN-L compounds (Cu to L).

Most of the CuSCN-L complexes show modest emission temperature dependence, which has been seen in many low-dimensional materials of closed-shell transition metals.[27] The emission red shift as the temperature decreases from room temperature to 77 K is due to the stacked metal−metal distance contraction. The long lifetime emission peaks are due to a ^{3}MLCT, in which the HOMO derives from the interaction between copper d_{z^2}, and the amine LUMO which is largely π^*. The contraction of the Cu···Cu distance favors electron coupling and leads to the decrease of the HOMO−LUMO gap; therefore, the emission red shifts at lower temperature. The only exception is $CuSCN(3ClPy)_2$, complex **11a**. This is due to a decrease in C···Cl separation where the electronegative Cl raises the energy of the LUMO and decreases the electron coupling, leading to an increase of the energy gap, resulting in a blue shift in the emission peak at 77 K.

CONCLUSIONS

We have reported the facile reaction of various neat liquid amines with solid copper(I) thiocyanate to produce amine-decorated CuSCN networks. In several cases multiple CuSCN:L stoichiometries were noted. Compounds having CuSCN/L ratios of 1:2 are zigzag or helical chains decorated with amines. When the ratio is 1:1 the products usually have ladder or sheet structures as a result of S,S,N-thiocyanate bridging. However, when the amine is a 2,6-disubstituted pyridine, (CuSCN)L chains are produced, with 3-coordinate copper. 3-Ethylpyridine produces an unusual monomeric $(CuSCN)L_3$ product with terminal N-bound SCN. In all cases, the amines are readily removed with heating. The $(CuSCN)L_2$ complexes with L = substituted pyridine are photoluminescent, showing excitation in the near UV and a broad emission near the yellow-green region. Microsecond lifetimes suggest phosphorescence behavior. Absence of photoemission in all species with aliphatic amine ligands suggests the importance of π^*-acceptor orbitals.

ASSOCIATED CONTENT

Supporting Information. (1) X-ray powder patterns (experimental and calculated) for all structurally characterized compounds. (2) TGA traces for all compounds. (3) Additional luminescence spectra for all luminescent compounds. (4) Luminescence photos for all emissive compounds and for the **1a** → **1b** conversion. (5) DFT calculated orbital energy table and isodensity maps. This material is available free of charge via the Internet at http://pubs.acs.org.

AUTHOR INFORMATION

Corresponding Author

*Phone: 757-2212555. Fax: 757-2212715. E-mail: rdpike@wm.edu.

ACKNOWLEDGMENT

Grateful acknowledgement is made to National Science Foundation (CHE-0848109 and CHE-0315877) for support of this research. We also acknowledge a Howard Hughes Medical Institute grant through the Undergraduate Biological Sciences Education Program to the College of William and Mary. We are indebted to NSF (CHE-0443345) and the College of William and Mary for the purchase of the X-ray equipment.

REFERENCES

(1) (a) Tronic, T. A.; deKrafft, K. E.; Lim, M. J.; Ley, A. N.; Pike, R. D. *Inorg. Chem.* **2007**, *46*, 8897–8912. (b) Pike, R. D.; deKrafft, K. E.; Ley, A. N.; Tronic, T. A. *Chem. Commun.* **2007**, 3732–3734. (c) Lim, M. J.; Murray, C. A.; Tronic, T. A.; deKrafft, K. E.; Ley, A. N.; deButts, J. C.; Pike, R. D.; Lu, H.; Patterson, H. H. *Inorg. Chem.* **2008**, *47*, 6931–6947.

(2) (a) Ley, A. N.; Dunaway, L. E.; Brewster, T. P.; Dembo, M. D.; Harris, T. D.; Baril-Robert, F.; Li, X.; Patterson, H. H.; Pike, R. D. *Chem. Commun.* **2010**, *46*, 4565–4567. (b) Dembo, M. D.; Dunaway, L. E.;

Jones, J. S.; Lepekhina, E. A.; McCullough, S. M.; Ming, J. L.; Li, X.; Baril-Robert, F.; Patterson, H. H.; Bayse, C. A.; Pike, R. D. *Inorg. Chim. Acta* **2010**, *364*, 102–114.

(3) Kabesova, M.; Boca, R.; Melnik, M.; Valigura, D.; Dunaj-Jurco, M. *Coord. Chem. Rev.* **1995**, *140*, 115–135.

(4) (a) Pereraa, V. P. S.; Senevirathnaa, M. K. I.; Pitigalaa, P. K. D. D. P.; Tennakone, K. *Sol. Energy Mater. Sol. Cells* **2005**, *86*, 443–450. (b) Dittrich, T.; Kieven, D.; Belaidi, A.; Rusu, M.; Tornow, J.; Schwarzburg, K.; Lux-Steiner, M. C. *J. Appl. Phys.* **2009**, *105*, 034509−1–034509−6. (c) Jaffe, J. E.; Kaspar, T. C.; Droubay, T. C.; Varga, T.; Bowden, M. E.; Exarhos, G. J. *J. Phys. Chem. C* **2010**, *114*, 9111–9117.

(5) (a) Kabesova, M.; Dunaj-Jurco, M.; Serator, M.; Gazo, J. *Inorg. Chim. Acta* **1976**, *17*, 161–165. (b) Smith, D. L.; Saunders, V. I. *Acta Crystallogr., Sect. B* **1981**, *37*, 1807–1812. (c) Smith, D. L.; Saunders, V. I. *Acta Crystallogr., Sect. B* **1982**, *38*, 907–909.

(6) (a) Dessy, G.; Fares, D.; Imperatori, P.; Morpurgo, G. O. *J. Chem. Soc., Dalton Trans.* **1985**, 1285–1288. (b) Wang, Q.-M.; Guo, G.-C.; Mak, T. C. W. *Chem. Commun.* **1999**, 1849–1850. (c) Blake, A. J.; Brooks, N. R.; Champness, N. A.; Crew, M.; Hanton, L. R.; Hubberstey, P.; Parsons, S.; Schröder, M. *Dalton Trans.* **1999**, 2813–2817. (d) Teichert, O.; Sheldrick, W. S. *Z. Anorg. Allg. Chem.* **1999**, *625*, 1860–1865. (e) Barnett, S. A.; Blake, A. J.; Champness, N. A.; Wilson, C. *CrystEngComm* **2000**, *5*, 36–40. (f) Teichert, O.; Sheldrick, W. S. *Z. Anorg. Allg. Chem.* **2000**, *626*, 2196–2202. (g) Näther, C.; Jess, I.; Kowallik, P. *Z. Anorg. Allg. Chem.* **2003**, *629*, 2144–2151. (h) Näther, C.; Greve, J.; Jess, I.; Wickleder, C. *Solid State Sci.* **2003**, *5*, 1167–1176. (i) Xu, Y.; Ren, Z.-G.; Li, H.-X.; Zhang, W.-H.; Chen, J.-X.; Zhang, Y.; Lang, J.-P. *J. Mol. Struct.* **2006**, *782*, 150–156. (j) Li, M.-X.; Wang, H.; Liang, S.-W.; Shao, M.; He, X.; Wang, Z.-X.; Zhu, S.-R. *Cryst. Growth Des.* **2009**, *9*, 4626–4633. (k) Yao, H.-G.; Zhou, P.; Ji, S.-H.; Ji, M.; An, Y.-L.; Ning, G.-L. *Z. Anorg. Allg. Chem.* **2009**, *635*, 2328–2332. (l) Ren, S.-B.; Yang, X.-L.; Zhang, J.; Li, Y.-Z.; Zheng, Y.-X.; Du, H.-B.; You, X.-Z. *CrystEngComm* **2009**, *11*, 246–248.

(7) (a) Saithong, S.; Pakawatchai, C.; Charmant, J. P. H. *Acta Crystallogr., Sect. E* **2007**, *63*, m857–m858. (b) Lobana, T. S.; Sharma, R.; Hundal, G.; Butcher, R. J. *Inorg. Chem.* **2006**, *45*, 9402–9409. (c) Bowmaker, G. A.; Hanna, J. V.; Skelton, B. W.; White, A. H. *Chem. Commun.* **2009**, 2168–2170.

(8) Bowmaker, G. A.; Hanna, J. V. *Z. Naturforsch. B* **2009**, *64*, 1478–1486.

(9) Toeniskoetter, R. H.; Solomon, S. *Inorg. Chem.* **1968**, *7*, 617–620.

(10) (a) Kromp, T.; Sheldrick, W. S.; Näther, C. *Z. Anorg. Allg. Chem.* **2003**, *629*, 45–54. (b) Näther, C.; Jess, I. *Acta Crystallogr., Sect. C* **2004**, *60*, m153–m155.

(11) Healy, P. C.; Pakawatchai, C.; Papasergio, R. I.; Patrick, V. A.; White, A. H. *Inorg. Chem.* **1984**, *23*, 3769–3776.

(12) Complex **3** (and its crystal structure), synthesized from Cu/thiourea/4MePy, has been re-reported: Harris, J. D.; Eckles, W. E.; Hepp, A. F.; Duraj, S. A.; Fanwick, P. E.; Richardson, J.; Gordon, E. M. *Mater. Des.* **2001**, *22*, 625–634.

(13) McGee, K. A.; Veltkamp, D. J.; Marquardt, B. J.; Mann, K. R. *J. Am. Chem. Soc.* **2007**, *129*, 15092–15093.

(14) Frisch, M. J.; Trucks, G. W.; Schlegel, H. B.; Scuseria, G. E.; Robb, M. A.; Cheeseman, J. R.; Zakrewski, V. G.; Montgomery, J. A., Jr.; Stratmann, R. E.; Burant, J. C.; Dapprich, S.; Millam, J. M.; Daniels, A. D.; Kudin, K. N.; Strain, M. C.; Farkas, O.; Tomasi, J.; Barone, V.; Cossi, M.;Cammi, R.; Mennucci, B.; Pomelli, C.; Adamo, C.; Clifford, S.; Ochterski, J.; Petersson, G. A.; Ayala, P. Y.; Cui, Q.; Morokuma, K.; Malick, D. K.; Rabuck, A. D.; Raghavachari, K.; Foresman, J. B.; Cioslowski, J.; Ortiz, J. V.; Baboul, A. G.; Stefanov, B. B.; Liu, G.; Liashenko, A.; Piskorz, P.;Komaromi, I.; Gomperts, R.; Martin, R. L.; Fox, D. J.; Keith, T.; Al-Laham,M. A.; Peng, C. Y.; Nanayakkara, A.; Challacombe, M.; Gill, P. M. W.; Johnson, B.; Chen, W.; Wong, M. W.; Andres, J. L.; Gozalez, C.; Head-Gordon, M.; Replogle, E. S.; Pople, J. A. *Gaussian '03*, Revision C.02; Gaussian, Inc.: Wallingford, CT, 2003.

(15) (a) Becke, A. D. *J. Chem. Phys.* **1993**, *98*, 5648–5652. (b) Lee, C.; Yang, W.; Parr, R. G. *Phys. Rev. B* **1988**, *37*, 785–789.

(16) *SMART Apex II, Data Collection Software*, version 2.1; Bruker AXS Inc.: Madison, WI, 2005.

(17) *SAINT Plus, Data Reduction Software*, version 7.34a; Bruker AXS Inc.: Madison, WI, 2005.

(18) Sheldrick, G. M. *SADABS*; University of Göttingen: Göttingen, Germany, 2005.

(19) Sheldrick, G. M. *Acta Crystallogr., Sect. A* **2008**, *64*, 112–122.

(20) *DIFFRAC Plus*, version 10.0 and *EVA*, release 2004; Bruker AXS Inc.: Madison, WI, 2005.

(21) *Crystallographica*, version 1.60d; Oxford Cryosystems Ltd.: Oxford, U.K., 2007.

(22) (a) Pyykkö, P. *Chem. Rev.* **1997**, *97*, 597–636. (b) Hermann, H. L.; Bosch, G.; Schwerdtfeger, P. *Chem.—Eur. J.* **2001**, *7*, 5333–5342.

(23) Baer, C.; Pike, J. *J. Chem. Educ.* **2010**, *87*, 724–726 and references cited therein.

(24) Bayse, C. A.; Brewster, T. P.; Pike, R. D. *Inorg. Chem.* **2009**, *48*, 174–182.

(25) (a) Ford, P. C.; Cariati, E.; Bourassa, J. *Chem. Rev.* **1999**, *99*, 3625–3647. (b) Araki, H.; Tsuge, K.; Sasaki, Y.; Ishizaka, S.; Kitamura, N. *Inorg. Chem.* **2007**, *46*, 10032–10034.

(26) Armaroli, N.; Accorsi, G.; Cardinali, F.; Listorti, A. *Top. Curr. Chem.* **2007**, *280*, 69–115.

(27) (a) Gliemann, G.; Yersin, H. *Struct. Bonding (Berlin)* **1985**, *62*, 87–153. (b) Connick, W. B.; Henling, L. M.; Marsh, R. E.; Gray, H. B. *Inorg. Chem.* **1996**, *35*, 6261–6265.